

www.scichina.com earth.scichina.com www.springerlink.com

Forest NPP estimation based on MODIS data under cloudless condition

CHEN LiangFu^{1,2†}, GAO YanHua^{1,3}, LI Li¹, LIU QinHuo^{1,2} & GU XingFa^{1,2}

Based on light-use efficiency model, an MODIS-derived daily net primary production (NPP) model was developed. In this model, a new model for the fraction of photosynthetically active radiation absorbed by vegetation (FPAR) is developed based on leaf area index (LAI) and albedo parameters, and a photosynthetically active radiation (PAR) is calculated from the combination of Bird's model with aerosol optical thickness and water vapor derived from cloud free MODIS images. These two models are integrated into our predicted NPP model, whose most parameters are retrieved from MODIS data. In order to validate our NPP model, the observed NPP in the Qianyanzhou station and the Changbai Mountains station are used to compare with our predicted NPP, showing that they are in good agreement. The NASA NPP products also have been downloaded and compared with the measurements, which shows that the NASA NPP products underestimated NPP in the Qianyanzhou station but overestimated in the Changbai Mountains station in 2004.

MODIS, net primary production, fraction of photosynthetically active radiation, photosynthetically active radiation

Among the missing carbon sink problems^[1,2], terrestrial ecosystems are recognized as the biggest unknown field^[3]. Thus, to determine the role of terrestrial ecosystems in the global carbon cycle and understand its shortand long-term dynamics are of high practical and scientific importance. Remote sensing has been paid increasingly more attention regarding the regional or global scale net primary production (NPP) estimation. For example, the vegetation index (VI) and leaf area index (LAI) retrieved from satellite images have been used as inputs in different terrestrial ecosystem models^[4–7]. The light-use efficiency model^[8] elaborated by Monteith has been widely used to estimate NPP based on remote sensing data^[9–11]. In light-use efficiency models based on remote sensing images, NPP can be expressed as

$$NPP = \varepsilon_{n} \times f_{PAR} \times Q_{PAR}, \qquad (1)$$

where ε_n is the light-use efficiency; f_{PAR} is the fraction of incident photosynthetically active radiation (PAR) ab-

sorbed by vegetation and Q_{PAR} is photosynthetically active radiation.

The $Q_{\rm PAR}$ is the solar radiation incidence between 400 and 700 nm that reached the surface after attenuation by atmospheric scattering, being absorbed from the top of the atmosphere. The $Q_{\rm PAR}$ is simply calculated to be 43–44 percent of total incident shortwave radiation measured by weather station and interpolated into the regional scale based on measurements from the limited number of weather stations [6,11,12], and interpolation can bring errors into model especially in large area where there are no climate stations or only several stations. In fact, $Q_{\rm PAR}$ is relative to the angle of solar incidence and atmosphere state, especially the atmospheric aerosol

Received July 4, 2007; accepted September 19, 2007

doi: 10.1007/s11430-008-0013-8

[†]Corresponding author (email: <u>Lfchen@irsa.ac.cn</u>)

Supported by the National Basic Research Program of China (Grant No. 2002CB412506) and the National Natural Science Foundation of China (Grant No. 40471092)

¹ State Key Laboratory of Remote Sensing Science jointly sponsored by Institute of Remote Sensing Applications of Chinese Academy of Sciences and Beijing Normal University, Beijing 100101, China;

² The Center for National Spaceborne Demonstration, Chinese National Space Administration, Beijing 100101, China;

³ Institute of Geographic Sciences and Natural Resources Research, Chinese Academy of Sciences, Beijing 100101, China

optic thickness and water vapor content. The specific atmospheric water and aerosol conditions must be taken into account for the total and spectral irradiance computation.

Fraction of photosynthetically active radiation absorbed by vegetation (FPAR) is a very important parameter in the NPP model. For the existing remote sensing NPP models, FPAR is calculated respectively from the Normalized Difference Vegetation Index (NDVI) used in Glo-PEM NPP model^[9] and Enhanced Vegetation Index (EVI) in VMP model^[11], so it is affected by VI characteristics. VI varies with view angle and sensors bands. In fact, according to its definition, FPAR only depends on the solar incident angle and the canopy parameters.

Accordingly, it is necessary to develop better models to retrieve PAR and FPAR directly from remote sensing measurements to improve the NPP estimation precision. In order to address these issues, the MODIS data are used in our model because of its good quality and multi-band, Otherwise, the MODIS NPP product can be used to compare with our NPP model results, and the flux tower measurements were used to validate NPP model. In this paper, the second section is the details of the algorithms of FPAR and PAR calculation, and the inversion methods of all the parameters used in the FPAR and PAR model. The third section is the model test site description, MODIS data processing, the ground-based LAI measurements and LAI inversion from MODIS data. In the fourth part of the article, we showed the inversion results of the specific parameters from MODIS data. We also have shown a comparison between the NPP results from our model, MODIS NPP product and the flux tower NPP measurements.

1 MODIS-derived NPP model and its parameterization

1.1 MODIS-derived NPP model

The MODIS-derived NPP model in this paper is described by eq. (1), FPAR and PAR algorithms are the most important parts in this model. FPAR is the fraction of solar radiation absorbed by canopy, which can be calculated using the following equation according to energy budget balance principle,

$$f_{\text{PAR}} = 1 - p_{\text{gap}} - \alpha, \tag{2}$$

where $p_{\rm gap}$ is canopy gap probability, expressed as

$$P_{\rm gap} = \exp\left[-\text{LAI} \cdot \Omega(\theta_{\rm s}) \cdot G(\theta_{\rm s}) / \mu_{\rm s}\right],\tag{3}$$

where $\Omega(\theta_s)$ and $G(\theta_s)$ are respectively assembled indices of foliage and attenuation coefficients in the solar zenith angle θ_s . In this paper, $\Omega(\theta_s)$ is assumed to be "1" for the random distribution of the foliage and μ_s is the cosine of θ_s . α in eq. (2) is the albedo, including the canopy and the background scattering, which is integrated from 400 to 700 nm. Eq. (2) shows that the FPAR can be underestimated because all the scattering photons by the background will be intercepted and absorbed again by the canopy when it rebounds up towards the canopy. So, in this paper, the FPAR in eq. (2) at canopy-level is modified as

$$f_{\text{PAR}} = 1 - p_{\text{gap}} - \alpha + p_{\text{gap}} \alpha_{\text{b}} (1 - K_{\text{open}}), \tag{4}$$

where α_b represents the background albedo, including soil or litter surface, and it is also integrated from 400 to 700 nm. K_{open} is the openness of the crown at the top of canopy, describing how much PAR there scatterred by the ground is passing through the crown to the top of the canopy. K_{open} is expressed as^[13]

$$K_{\text{open}} = \int_{0}^{\pi/2} p_{\text{gap}}(\theta) \sin 2\theta d\theta.$$
 (5)

The multi-scattering in crown and multi-responding between the crown and background have been taken into account in eq. (5).

PAR model from remote sensing measurements can provide PAR spatial distribution with 1 km resolution. The total downwelling spectral surface irradiance includes two parts of the irradiance. One is direct irradiance, which is not scattered, but proceeds directly to the surface of the earth after losses by absorption, the other is diffuse irradiance, which is scattered out of the direct beam, and towards the surface. It can be described by

$$E(\lambda) = E_{d}(\lambda) + E_{s}(\lambda), \tag{6}$$

where the subscripts d and s represent direct and diffuse components, respectively. The attenuation of solar irradiance in the visible and near-infrared wavelengths comprises the following atmospheric processes: absorption by ozone, the gas mixture (primarily by oxygen), water vapor and scattering, scattering by the gas mixture (Rayleigh scattering), and aerosols. The water vapor and aerosol can be retrieved from MODIS data, and their inversion methods will be described later in this paper. The first step in this PAR algorithm is to compute the downwelling irradiance just above the land surface at 1 nm resolution and 1 km spatial resolution.

Here, the diffuse component should be emphasized, which can be described by

$$E_{\rm s}(\lambda) = I_{\rm r}(\lambda) + I_{\rm a}(\lambda) + I_{\rm g}(\lambda), \tag{7}$$

where I_r , I_a , and I_g respectively represent the diffuse components of incident irradiance arising from Rayleigh scattering, aerosol scattering and multiple ground-air interactions. The multiple ground-air interactions must be taken into account in the diffuse component, being a function of land surface albedo. For the land surface, this part can be expressed as

$$I_{g} = E_{d} \cdot \alpha_{BSA} \cdot r + (I_{r} + I_{a}) \cdot \alpha_{WSA} \cdot r + \left[E_{d} \cdot \alpha_{BSA} \cdot r + (I_{r} + I_{a}) \cdot \alpha_{WSA} \cdot r \right] + \frac{\left[E_{d} \cdot \alpha_{BSA} \cdot r + (I_{r} + I_{a}) \cdot \alpha_{WSA} \cdot r \right]}{1 - \alpha_{WSA} \cdot r},$$
(8)

where α_{BSA} and α_{WSA} are respectively black-sky albedo and white-sky albedo, and r is atmospheric albedo.

Owing to only three visible bands (459–479, 545–565, and 620–670 nm) ranging from 400 to 700 nm can be used to calculate the PAR, the instantaneous photosynthetically available radiation (IPAR) is integrated by using a weighted sum at each of the three visible MODIS wavebands. Finally, a daily PAR is integrated. The solar radiative spectrum on the top of atmosphere used in this article was obtained from the World Radiation Center^[14].

In eq. (1), the light-use efficiency
$$\varepsilon_n$$
 is expressed as
$$\varepsilon_n = \varepsilon_0 \times f(T) \times f(W), \qquad (9)$$

where ε_0 is the maximum light-use efficiency in optimal condition, f(T) and f(W) are air temperature and plant water stresses on the photosynthesis in the terrestrial ecosystem. ε_0 is a very important coefficient in the model. It is unreasonable to set one constant to ε_0 just like the CASA model. In this paper, the maximum light-use efficiency model is cited from Glo-PEM model^[9]. In eq. (9) daily averaged air temperature is taken into account to limit the photosynthesis according to the air temperature function in the Biome-BGC model^[10], and this function is

$$f(T) = \begin{cases} \frac{\log(T+1)}{\log(T_{\text{opt}}+1)}, & T < T_{\text{opt}} \\ \cos\left(\frac{T-T_{\text{opt}}}{T_{\text{max}}-T_{\text{opt}}} \times \frac{\pi}{2}\right), & T \ge T_{\text{opt}} \end{cases}$$

$$0, & T < 0$$
(10)

where $T_{\rm opt}$ is the optimal temperature for plant's growth; $T_{\rm max}$ is the maximum temperature and is often set to be

 40° C. The f(W) is cited from the VMP model^[11], which is expressed as

$$f(W) = \frac{1 + LSWI}{1 + LSWI_{max}},$$
(11)

where LSWI is calculated based on near-infrared band reflectance, that is,

LSWI =
$$(\rho_{\text{nir}} - \rho_{\text{swir}})/(\rho_{\text{nir}} + \rho_{\text{swir}}),$$
 (12)

where ρ_{hir} and ρ_{swir} are MODIS reflectances of near-infrared bands, 841-875 and 1628-1652 nm. LSWI_{max} in eq. (11) is maximum land surface water index during the whole plant growth.

1.2 Parameterization method of the MODIS-derived NPP model

In the MODIS-derived NPP model, the light-use efficiency, FPAR, and PAR all depend on both the reflectance of the land surface and the atmospheric condition. Several related parameters in the model need to inverse from MODIS data, such as the atmospheric water vapor and aerosol retrievals, the BRDF, albedo and LAI. Here are the brief descriptions of the inversion methods used in this MODIS-derived NPP model.

After discriminating cloud-free pixel from image with the MODIS cloud detecting algorithm, the atmospheric water vapor and aerosol were first retrieved from MODIS cloud-free pixels. The total vertical amount of water vapor can be derived using a comparison way between the reflected solar radiation in the absorption channels and in the nearby non-absorption channel [15]. Aerosol optical depth is often retrieved based on the dark object algorithm because the reflectance of dense vegetation and water in near-IR field is very low and the sensor signal is mainly from the scattering of atmospheric aerosol. A reflectance model for sparse lookup tables based on the 6S code is often used, whose aerosol optical depth can be retrieved based on the 6S code [16]. In this article, the surface reflectance models for dense and sparse vegetation are used to separate the surface reflection contribution from the satellite-received radiance, and then the aerosol optical thickness is retrieved based on a lookup table based on the 6S code.

Albedo is defined as the ratio of upwelling to down-welling radiation flux on the surface. Downwelling flux may be written as the sum of a direct component and a diffuse component. Black-sky albedo is defined as albedo in the absence of a diffuse component and is a function of solar zenith angle. White sky albedo is de-

fined as albedo in the absence of a direct component when the diffuse component is isotropic. Albedo from the BRDF model, which is called a kernel-based BRDF model^[17], can be expressed as

BRDF =
$$f_{\text{iso}} + f_{\text{geo}}k_{\text{geo}} + f_{\text{vol}}k_{\text{vol}}$$
, (13)

where k_{geo} , k_{vol} respectively represent a geometric optical kernel and a radiation transfer kernel, f_{iso} , f_{geo} , f_{vol} are model parameters, denoted as f_n , n represents the different subscripts. The channel black-sky and white-sky albedos are given by

$$a_{\text{BSA}}(i) = \sum_{n} f_n(i) h_n(\theta), \tag{14}$$

$$a_{\text{WSA}}(i) = \sum_{n} f_n(i) H_n, \qquad (15)$$

where the i means the channel, the kernel integrals h_n and H_n do not depend on the observations, they may therefore be pre-computed based on the definition as follows:

$$h_n(\theta) = \frac{1}{\pi} \int_0^{2\pi} \int_0^{\pi/2} k_n(\theta, \theta, \phi) \sin(\theta) \cos(\theta) d\theta d\phi, \qquad (16)$$

$$H_n = 2 \int_0^{\pi/2} h_n(\theta) \sin(\theta) \cos(\theta) d\theta. \tag{17}$$

Note that $k_n(\theta, \theta, \phi)$ is the kernel function. Based on the narrow channel albedo, the visible width band black-sky albedo α_{BSA} and white-sky albedo α_{WSA} can be integrated using the model present in ref. [18].

LAI is an important structural property of plant canopy, which is defined as the one-sided leaf area per unit ground area. One of the simplest ways to retrieve LAI is based on the relationship between the vegetation index and leaf area index^[19]. NDVI and SR are most widely used to derive LAI^[4,10]. But for continual vegetation canopies, physical models are mainly used to simulate the canopy reflectance and to obtain LAI, such as the SAIL (scattering by arbitrarily inclined leaves) model for the continuous canopy^[20]. In our NPP model, the crop and grass LAI is derived from the SAIL model, but for forest the LAI is calculated based on the correlation between the vegetation index and the measured LAI^[21].

The MODIS-derived NPP model flow chart is showed in Figure 1.

2 Test site and data processing

2.1 Test site

We chose two test sites to validate our NPP model. They

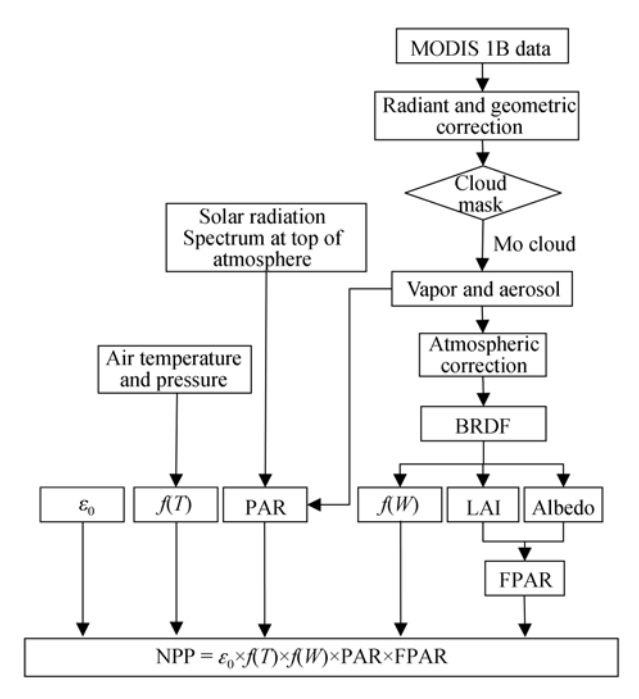


Figure 1 MODIS-based NPP model flow sketch. In this paper, the FPAR, PAR and f(W) are all retrieved from the MODIS data and f(T) from measurements.

are Qianyanzhou Ecological Experimental Station and Changbai Mountains Ecological Experimental Station, which all belong to Chinese Ecosystem Research Network (CERN).

Qianyanzhou station is located in the mid-subtropical monsoon landscape zone of South China. The artificial coniferous forest was planted in middle 1980s. The flux tower (115°03′29.2″E, 26°44′29.1″N), set up in 2002, is located at the top of a hill, in a hilly topography with a slope ranging between 2.8° and 13.5°. The forest coverage is about 90% around the tower, with slash pine in the west, masson pine in the southeast, and Chinese fir dominating in the northeast. The Changbai Mountains station is situated in the northern slope of Changbai Mountains, in Jilin Province, at latitude 42°4'N, longitude 128°8'E, and with an altitude of 736 m. In each station, the flux tower is set to attach the eddy covariance system including routine meteorology systems, open-path eddy covariance and synchronous closed-path eddy covariance measurement. The two eddy covariance systems consist of three-dimensional sonic anemometers (CSAT3, Campbell Scientific Ltd, USA) to record wind speed and temperature, and of an infrared gas analyzer (Li-7500, Li Corporation Inc, USA) for measuring CO₂ and water vapor concentrations. In addition, the routine meteorological system provides the measurements of global radiation, net radiation, PAR sensors, infrared thermometer, soil temperature sensors, soil moisture sensors, and soil heat flux plate. The details of flux tower introduction and flux arithmetic can be found in ref. [22].

2.2 Acquisition and processing of MODIS data

The MODIS data are the key data source to simulate the NPP using this model. We login the MODIS/Terra Multiple Data Ordering Page to download the 1-km resolution L1B MODIS data for our study sites. There are 65 days in 2003 and 2004 cloud-free images for Qianyanzhou station and only 14 d for Changbai Mountains station in 2004.

2.3 Ground-based LAI measurements and LAI inversion from MODIS

For the Qianyanzhou forest region, the correlation between vegetation index and LAI is used. We chose 30 stands, of which 13 are located in the Qianyanzhou station region, while the other auxiliary sites are scattered along two different transects, which extend several kilometers away from the Qianyanzhou station. The LAI measurements using TRAC (Tracing Radiation and Architecture of Canopies)[6,18] were made during the clear days from October 27 to November 5, 2003. Because it is not easy to find a 100 m or even wide enough place to extend the long transect at the hillside, two or three parallel transects of equal length, 40-60 m, are designed at each site. All transects are located 5-10 m apart and oriented in the direction perpendicular to solar azimuth. The TRAC measurements were made along transect. Because of the dense vegetation under the Pinus massoniana and the thin Pinus elliottii forests, LAI under canopy can not be measured by TRAC, and we made 2 or 3 samples with 1 m×1 m size and measured all the leaves areas of grass and shrubs in each sample using digital photos. The total LAI in these forest is the sum of the ground sample measurement and TRAC measurement.

In order to develop the relationship between LAI ground measurements and the MODIS vegetation index, the high resolution image Landsat TM with 30 m and Gauss Kruger 20 map projection at GM starting time 02:23:09 on October 26 in 2003 is chosen, and then the relationship will be scaled up to MODIS data with a 1 km resolution. LANDSAT-5 TM is registered using over 40 ground control points obtained from 1:50000

maps and the digital elevation model. The registration accuracy was within ±1 pixel (±30 m). Radiometric corrections were then made using gained and offset coefficients provided by the images. The atmospheric corrections using 6S were made to convert the radiance measurements at the top of the atmosphere to the surface-level reflectance for further simple SR calculation. Then, we obtained the linear relationship between SR index from TM image and LAI measured from 30 stands. In order to make this relationship available for coarse MODIS data, the reflectance of red channel and near infrared channel of TM image are scaled up to a 1 km spatial resolution by averaging every 33×33 pixel's values. The linear relationship is shown in Figure 2.

With the same method, the relationship between LAI and VI has been obtained after the field experiments in Changbai Mountains station. Here, we directly cite the result from ref. [23].

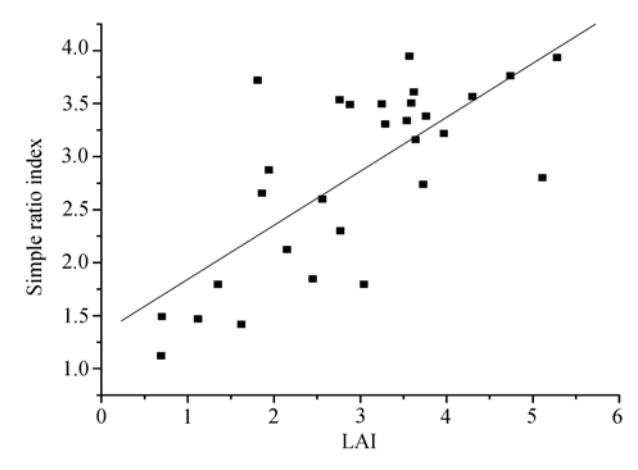


Figure 2 The linear relationship between ground measurements of LAI and simple ratio index from Landsat-5 TM image. It can be fit for a linear relation LAI= $0.50907 \times SR+1.33445$. LAI ground measurement samples are 29, R is 0.72684, and SD is 0.60116 for the linear regression between LAI and a simple ratio index.

2.4 Meteorological parameters

The NPP calculation from MODIS in this paper requires several meteorologic parameters, such as the daily average air temperature, air pressure, and air relative humidity. The daily average air temperature is calculated from the average of daily maximum and minimum air temperatures measured by the flux tower measurement system. When our NPP model is used to calculate the NPP on region scale or larger area scale, the interpolation meteorologic data measured from climate station can be used in eq. (9).

2.5 The simulation of the MODIS-derived NPP model

In this paper, cloud free MODIS L1B data are downloaded and processed according to the flow chat in Figure 1. Then, the parameters related to the NPP model mentioned above are retrieved. Finally, the daily NPP model on the day scale is conducted using MODIS-derived parameters and metrological data. In order to validate model results with the observed NPP on the stand scale, the retrieved parameters and NPP values of the pixel located at the Changbai Mountains and Qianyanzhou stations flux towers are picked up from the image and shown in the following section.

3 Results

3.1 The comparison between retrieved PAR and observed PAR

In order to validate our albedo algorithm used in this paper, we use the 16-day MODIS data in North China to get the albedo and compare it with the NASA albedo product. It shows that our albedo is consistent with NASA albedo product.

In order to validate the PAR algorithm, 54-day cloud-free MODIS data in 2003 and 2004 were processed, and the PAR of the pixel located at the Qianyanzhou station flux tower stand was calculated using the algorithm based on MODIS land surface reflectance, derived aerosol and water vapor content, combined with air pressure measured by the climate station. The measured PAR at the Qianyanzhou station flux tower as ground true was used to compare with the predicted PAR. The results in Figure 3 show that the calculated daily PAR is consistent with the observed PAR, where the linear correlation coefficient between the calculated and the observed PAR is 0.93, even though the spatial scale is different for 1-km pixel for calculated PAR and flux tower stand for observed PAR.

3.2 Results of MODIS-derived NPP simulation

In order to validate MODIS-derived NPP results, we compare the calculated NPP with the observed NPP from an eddy covariance system at the flux tower in the Qianyanzhou station and the Changbai Mountains station. The NPP values of the corresponding pixels, in which the flux tower was located, were picked up according to the geographical location of flux towers. The NASA daily NPP products in 2003 and 2004 for the two

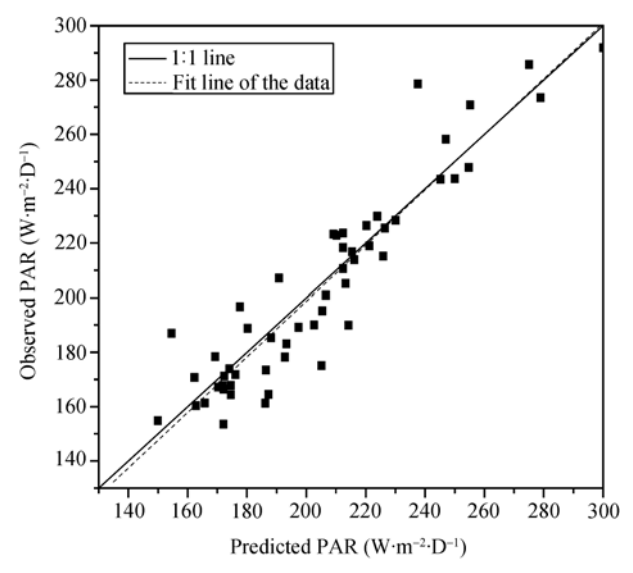


Figure 3 The comparison of the calculated PAR with the measured one at Qianyanzhou ecological experimental station in Jiangxi Province of South China. The simulated IPAR in this figure is picked out of the pixel from the flux tower located in 54-day cloud free MODIS images. The linear correlation coefficient between the calculated IPAR and the observed IPAR is 0.93, and SD is 13.19.

stations were downloaded for comparison. The results are shown in Figures 4 and 5. Though most of the observed NPP from June to August was absent in the two years, the results can also reveal the NPP trends. Figure 4(a) shows a good agreement between the predicted NPP product and NASA NPP product in 2003, and both of them are a little bit higher than their measurements. Figure 4(b) shows a very good consistency between the predicted NPP and observed NPP in 2004. We loaded the NASA daily NPP product down from the end of March in 2006 (from http://edcimswww.cr.usgs.gov/ pub/imswelcome/). The NASA daily NPP product in 2004 varied more smoothly than the observed NPP, and is too low during summer. Figure 5 shows the comparison between the predicted daily NPP, NASA daily NPP product and daily observed NPP in 2004 at the Changbai Mountains station. The predicted NPP is coincident with the observed NPP, but the NASA daily NPP product is much higher than the observed NPP.

4 Discussions and conclusions

Generally speaking, through the comparison with the observed NPP at the Qianyanzhou station and Changbai Mountains station in 2003 and 2004, our MODIS-derived NPP model is feasible. It can provide the NPP distribution with 1 km spatial resolution.

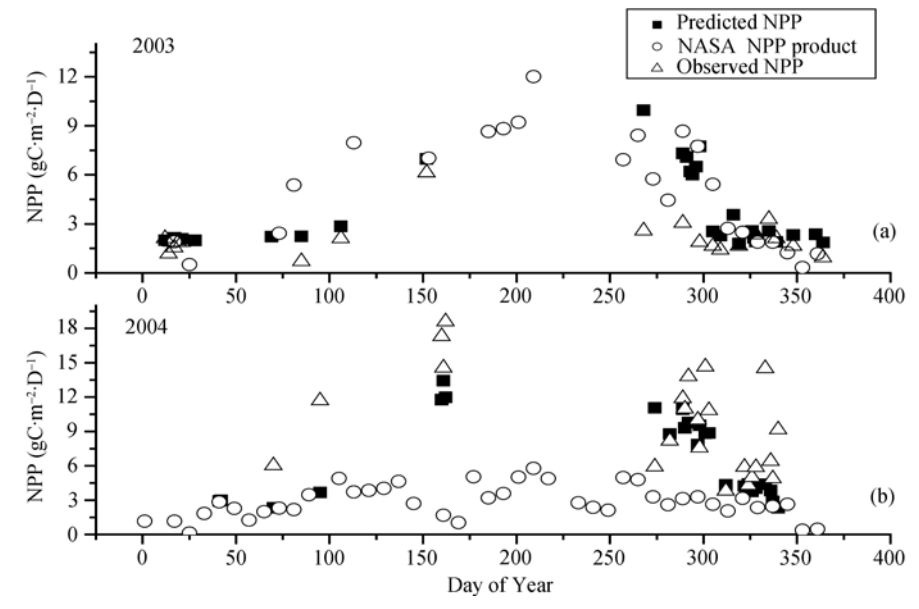


Figure 4 A comparison between calculated NPP, observed NPP, and NASA NPP product. Two-year results were used. The black rectangles represent the predicted NPP, the triangles represent the observed NPP, and the circles are the NASA NPP product. We loaded the NASA NPP product down in different years.

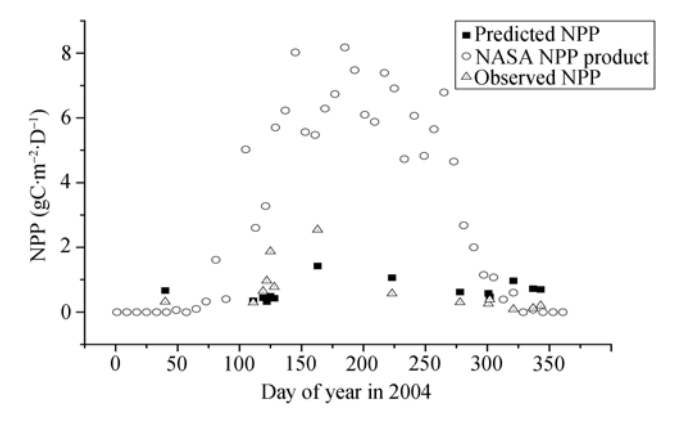


Figure 5 A comparison between the predicted daily NPP, NASA daily NPP product and daily observed NPP in 2004 at the Changbai Mountains station. The predicted NPP is coincident with the observed NPP, but the NASA daily NPP product is much higher than the observed NPP, which is much overestimated.

However, we know that there are uncertainties in its testing, because of the different spatial scales for the MODIS-derived NPP (1-km spatial scale) and observed NPP (stand scale) though the flux towers of the two stations is located in flat area. And footprint in the hilly region will bring uncertainties into the comparison.

The PAR model in our NPP algorithm can be used to provide the PAR regional distribution results, especially for the large area without any climate stations. It can eliminate the NPP error caused by the interpolation for large area with few measurements. Moreover, the factual atmospheric water vapor, aerosol optical thickness and the land surface albedo have been taken into account in

this model.

FPAR is a very important parameter in our NPP model. FPAR model in this paper is developed based on the energy balance principle, and the multi-scattering effects between the back-ground and crown have also been considered. The LAI and albedo are the key parameters in FPAR model, and they are independent of view angles, So this FPAR will not change with view angle, unlike the FPAR model based on vegetation index in Glo-PEM model^[9] and VMP model^[11].

There are also some uncertainties existing in this NPP model, because the NPP in this model is linear with the light-use efficiency, FPAR and PAR. So, any uncertainties brought about by parameters inverse from the MODIS data will incur effects on the final NPP value. In this paper, the light-use efficiency is not concerned, and we only focus on the development of FPAR and PAR model based on remote sensing data. How to get light-use efficiency on pixel scale from satellite image will be our next work.

In this paper, the NASA NPP products are also chosen to compare with the predicted results. The NASA NPP products in 2004 for the Qianyanzhou station and the Changbai Mountains station are not in good agreement with measurements, the NASA NPP product is less estimated at the Qianyanzhou station, but it is overestimated at the Changbai Mountains station.

The authors would like to thank the Chinese Ecosystem Research Network (CERN) for providing the observed data.

- 1 Broecker W S, Takahashi T, Simpson H H, et al. Fate of fossil fuel carbon dioxide and the global carbon budget. Science, 1979, 206: 409-418[DOI]
- 2 Tans P P, Fung I Y, Takahashi T. Observational constraints on the global atmospheric CO₂ budget. Science, 1990, 247: 1431—1438[DOI]
- 3 Houghton R A. Terrestrial sources and sinks of carbon inferred from terrestrial data. Tellus Ser B-Chem Phys Neteorol, 1996, 48: 420-432
- 4 Sellers P J, Meeson B W, Hall F G, et al. Prmote sensing of the land surface for studies of global change: Models-Algorithms-Experiments. Remote Sens Environ, 1995, 51(1): 3—26[DOI]
- 5 Schimal D S. Terrestrial biogeochemical cycles: Global estimates with remote sensing. Remote Sens Environ, 1995, 51(1): 49-56[DOI]
- 6 Chen J M, Liu J, Cihlar J, et al. Daily canopy photosynthesis model though temporal and spatial scaling for remote sensing applications. Eco Model, 1995, 124: 99—119[DOI]
- 7 Cao M K, Woodward F I. Dynamic responses of terrestrial ecosystem carbon cycling to global climate change. Nature, 1998, 393: 249-252[DOI]
- 8 Monteith J L. Solar radiation and productivity in tropical ecosystems. J Appl Ecol, 1972, 9: 747—766[DOI]
- 9 Prince S D, Goward S J. Global primary production: a remote sensing approach. J Biogeograph, 1995, 22: 815—835[DOI]
- 10 Running S W. Testing FOREST-BGC ecosystem process simulations across a climatic gradient in Oregon. Ecol Appl, 1994, 4(2): 238-247[DOI]
- Xiao X, Hollinger D, Aber J. Satellite-based modeling of gross primary production in an evergreen needle leaf forest. Remote Sens Environ, 2004, 89: 519-534[DOI]
- 12 Liu J, Chen J M, Cihlar J, et al. A process-based boreal ecosystem

- productivity simulator using remote sensing inputs. Remote Sens Environ, 1997, 62: 158-175[DOI]
- 13 Li X W, Wang J D. Vegetation Optical Remote Sensing Model and Parameterized Vegetation Structure (in Chinese). Beijing: Science Press 1995
- 14 Bird R, Riordan C. Simple solar spectral model for direct and diffuse irradiance on horizontal and tilted planes at the earth's surface for cloudless atmospheres. Amer Meteorol Soc, 1986, 25: 87-97
- 15 Kaufman Y J, Gao B C. Remote sensing of water vapor in the near IR from EOS/MODIS. IEEE Trans Geosci Remote Sensing, 1992, 30: 871-884[DOI]
- 16 Tanre P Y, Deschamps C D, Herman M. Estimation of Sahran aerosol optical thickness from blurring effects in Thematic Mapper data. J Geophys Res, 1998: 15955-15964
- 17 Gao F, Schaaf C, Strahler A H, et al. Using a multi-kernel least variance approach to retrieve and evaluate albedo from limited BRDF observations. Remote Sens Environ, 2001, 76: 57–66[DOI]
- 18 Liang S, Yu Y, Defelice T P. VIIRS narrowband to broadband land surface albedo conversion: Formula and validation. Int J Remote Sens, 2005, 26(5): 1019—1025[DOI]
- 19 Chen J M, Cihlar J. Retrieving leaf area index of boreal forests using Landsat TM images. Remote Sens Environ, 1996, 55: 153-162[DOI]
- 20 Verhoef W. Light scattering by leaf layers with application to canopy reflectance modeling: The SAIL model. Remote Sens Environ, 1984, 16: 125—141[DOI]
- 21 Liu Q H, Chen L F, Liu Q. Remote sensing inversion system. Version 1.0, 2003SR10784. 2003
- 22 Liu Y F, Song X, Sun X M, et al. Seasonal variation of CO₂ flux and its environmental factors in evergreen coniferous plantation. Sci China D-Earth Sci, 2005, 48(Suppl I): 123-132
- 23 Zhou Y. Measurement of LAI in Changbai mountains nature reserve and its result. Resour Sci (in Chinese), 2003, 25(6): 38-42